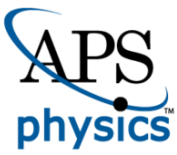

Operational Magic Intensity for Sr Optical Lattice Clocks

Ichiro Ushijima, Masao Takamoto, and Hidetoshi Katori

Phys. Rev. Lett. **121**, 263202 — Published 28 December 2018

DOI: 10.1103/PhysRevLett.121.263202

Operational Magic Intensity for Sr Optical Lattice Clocks

Ichiro Ushijima,[1,2] Masao Takamoto,[1,3] and Hidetoshi Katori[1,2,3]

[1]*Quantum Metrology Laboratory, RIKEN, Wako, Saitama 351-0198, Japan*
[2]*Department of Applied Physics, Graduate School of Engineering, The University of Tokyo, Bunkyo-ku, Tokyo 113-8656, Japan*
[3]*Space-Time Engineering Research Team, RIKEN, Wako, Saitama 351-0198, Japan*

(Dated: December 10, 2018)

We experimentally investigate the lattice-induced light-shift by the electric-quadrupole (E2) and magnetic-dipole (M1) polarizabilities and the hyperpolarizability in Sr optical lattice clocks. Precise control of the axial as well as radial motion of atoms in a one-dimensional lattice allows observing the E2-M1 polarizability difference. Measured polarizabilities determine an operational lattice-depth to be $72(2)E_R$, where the total light shift cancels to the 10^{-19} level, over lattice-intensity variation of about 30%. This operational trap depth and its allowable intensity range conveniently coincide with experimentally feasible operating conditions for Sr optical lattice clocks.

PACS numbers: 06.30.Ft, 32.60.+i, 37.10.Jk, 42.62.Eh

Recent progress of optical clocks has pushed their fractional uncertainty to the 10^{-18} level [1–4], which opens up new applications of clocks, such as chronometric geodesy [5, 6], tests of fundamental constants [7, 8], detection of dark matter [9] or gravitational waves [10]. Triggered by these advances, future redefinition of the second by optical clocks [11, 12] is in scope and its procedure is being discussed [13].

Better understanding and control of perturbations lies at the heart of continued progress of atomic clocks. Isolating atoms from electro-magnetic (EM) perturbations is of prime importance in designing ion clocks [14] where ions are confined nearly free from EM perturbations. Optical lattice clocks have shown that cancellation of trap perturbation leads to stable and accurate clocks with uncertainties less than 10^{-17} [2, 3, 12, 15], where the magic frequency aimed to equalize polarizabilities of the clock states so as to decouple the clock transition frequency from inhomogeneous trap perturbations [16]. Removal of perturbations by specifying the frequency is the essence of the optical lattice clock, which is based on the fact that the frequency is a precisely measurable quantity.

This magic frequency concept, however, becomes nontrivial for achieving inaccuracy of 10^{-18} because of non-negligible contribution of the higher-order light-shifts than that given by the electric-dipole (E1) interaction. In a standing wave of light, a quarter-wavelength spatial mismatch between the E1 potential and the potential induced by the electric-quadrupole (E2) and magnetic-dipole (M1) interactions introduces an atomic-motion-dependent light shift [17, 18]. In addition, the hyperpolarizability effect introduces a light shift proportional to the square of lattice intensity [16, 19]. Different spatial dependence makes these light shifts difficult to eliminate. An operational magic frequency [20] is proposed to compensate the higher order shifts by the E1 light shift and make overall light shift insensitive to lattice-intensity variation around a "magic intensity".

In order to find such operational condition, precise knowledge of the higher-order polarizabilities is mandatory. Higher-order light shifts have been investigated theoretically [21, 22] and experimentally for Sr [3, 11, 23], Yb [15, 24, 25] and Hg [26]. Recently, the hyperpolarizability is measured for Yb to find the operational magic frequency [15] with the help of a theoretical calculation of the E2-M1 polarizability. As for Sr, in spite of significant efforts, discrepancies between reported polarizabilities are not yet solved.

In this Letter, we investigate the hyperpolarizability and the E2-M1 polarizability for Sr atoms in a one-dimensional (1D) lattice. From the nonlinear intensity dependence of the light shift, we derive the hyperpolarizability. The E2-M1 polarizability is evaluated by measuring the light shift difference by changing the vibrational state of atoms in the lattice. Using the obtained polarizabilities, we derive two distinctive operational conditions that make the total light shift insensitive to lattice intensity variation at the 10^{-19} level.

The lattice-induced light shift $\nu_{\rm LS}$ is given by the light shift difference between the ground and excited states on the clock transition. For a 1D optical lattice as shown in Fig. 1(a), the light shift depends on the vibrational state n_z of atoms along the z-axis, the lattice laser intensity, and the detuning δ_L of lattice laser $\nu_L = \delta_L + \nu^{\rm E1}$ from the E1 magic frequency $\nu^{\rm E1}$ that makes the E1 polarizabilities $\alpha^{\rm E1}$ for the clock states equal. Since the peak intensity I_0 of the lattice is proportional to the trap depth $U \approx \alpha^{\rm E1} I_0$ (by neglecting the higher-order effects of less than 10^{-6}), we rewrite the light shift formula [20] in terms of a normalized trap depth $u = U/E_R$ with $E_R = (h\nu_L/c)^2/(2m)$ the lattice photon recoil energy as,

$$\begin{aligned} h\nu_{\rm LS}(u,\delta_L,n_z) \approx & \left(\tfrac{\partial\tilde{\alpha}^{\rm E1}}{\partial\nu}\delta_L - \tilde{\alpha}^{qm}\right)\left(n_z+\tfrac{1}{2}\right)u^{1/2} \\ & - \left[\tfrac{\partial\tilde{\alpha}^{\rm E1}}{\partial\nu}\delta_L + \tfrac{3}{2}\tilde{\beta}\left(n_z^2+n_z+\tfrac{1}{2}\right)\right]u \\ & + 2\tilde{\beta}\left(n_z+\tfrac{1}{2}\right)u^{3/2} - \tilde{\beta}\,u^2, \end{aligned} \tag{1}$$

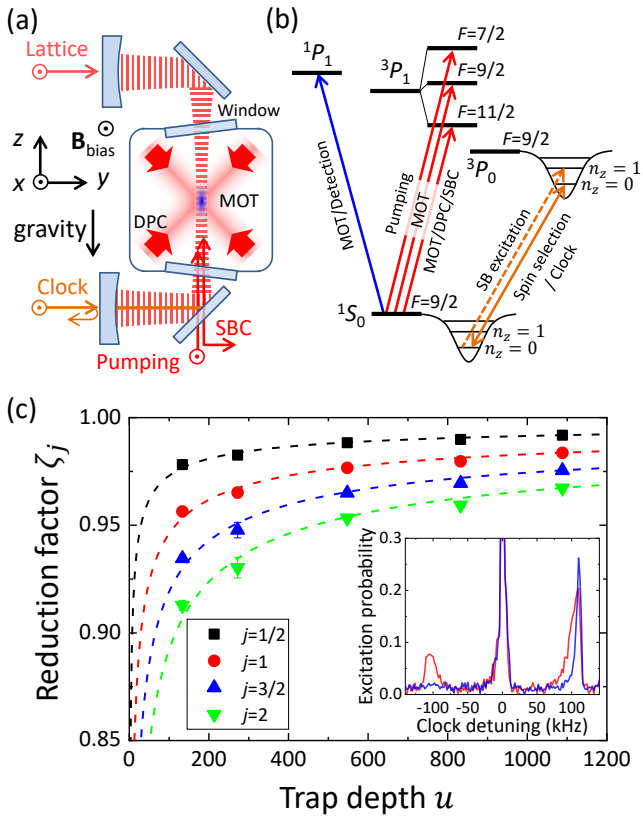

FIG. 1: (color online). (a) Experimental setup for the cavity-enhanced 1D lattice. After loading atoms from the magneto-optical trapping (MOT) into the lattice, we apply sideband cooling (SBC) and Doppler cooling (DPC) on the $^1S_0 - {}^3P_1$ transition. (b) Energy diagram for ^{87}Sr atoms. (c) Reduction factors ζ_j calculated from the radial temperature T_r are shown by symbols, where colors indicate j as given in the legend. The dashed lines show estimated reduction factors $\zeta_j^{\rm ad}(u)$ assuming the lattice depth is adiabatically varied from $u_{\rm ref} = 272$ (see text). The blue and red lines in the inset show motional sideband spectrum on the clock transition at $u_{\rm ref}$ with and without SBC/DPC.

where $\tilde{\alpha}^{\rm E1}$, $\tilde{\alpha}^{qm}$, and $\tilde{\beta}$ are the difference (denoted by tildes) of E1 and E2-M1 polarizabilities, and hyperpolarizability on the clock transition. The conversion of these polarizabilities are summarized in Supplemental Material [27]. While the light shift model given in Ref. [20] takes into account the anharmonicity of the lattice trap to $\mathcal{O}(z^4)$ in the axial coordinate expansion, we verify neglecting $\mathcal{O}(z^6)$ terms is valid for describing the light shift with low 10^{-19} uncertainty for Sr [27].

The lattice intensity is non-uniform in nature, as the spatial inhomogeneity itself is the essence of an optical trap. As the intensity critically affects the light shift as given in Eq. (1), precise control and evaluation of atomic distribution in the optical lattice is of particular importance. We consider atomic motion in the 1D lattice potential given by $\mathcal{U}(x,y,z) \approx -\alpha^{\rm E1} I_0 e^{-2(x^2+y^2)/w^2} \cos^2(2\pi z/\lambda_L)$, where I_0, w, and $\lambda_L = c/\nu_L$ are the peak intensity, the radius, and the wavelength of the lattice laser with a Gaussian profile. The axial and radial oscillation frequencies of atoms are given by $\nu_z = 2\sqrt{\alpha^{\rm E1} I_0 E_R/h}$ and $\nu_r = \nu_z \lambda_L/(\sqrt{2}\pi w) (\approx \nu_z/320$ for our experiment). In contrast to the axial vibrational states with averaged occupation $\bar{n}_z \approx 0$ that require quantum treatment, the radial motion can be treated classically as the vibrational states typically occupy $\bar{n}_r = k_{\rm B} T_r/(h\nu_r) \approx 110$ with T_r the radial temperature and $k_{\rm B}$ the Boltzmann constant. Assuming a thermal distribution $\rho(x,y) = \frac{m(2\pi\nu_r)^2}{2\pi k_B T_r} e^{-\frac{1}{2}m(2\pi\nu_r)^2(x^2+y^2)/(k_B T_r)}$ of atoms, the effective laser intensity experienced by the atoms is given by

$$\overline{u^j} = \int \rho(x,y) \left[\frac{\alpha^{\rm E1} I_0 e^{-2(x^2+y^2)/w^2}}{E_R}\right]^j dxdy \equiv \zeta_j u^j, \quad (2)$$

where we denote thermal average by bar and define a lattice-intensity reduction factor $\zeta_j(u) \approx 1 - \frac{j k_{\rm B} T_r}{u E_R}$. In the following, we evaluate the lattice light shifts of Eq. (1) by the effective intensity $\overline{u^j} = \zeta_j(u) u^j$.

To investigate the hyperpolarizability effect, we install a buildup cavity with a power enhancement factor of ≈ 20 for the 1D optical lattice oriented vertically as shown in Fig. 1(a). The beam radius is chosen as $w \approx 60$ μm to moderate atomic collisions and allows a maximum trap depth of $u \sim 1200$. This cavity also works as spatial filter to define a TEM$_{00}$ Gaussian mode. We use a Ti:sapphire laser at $\nu_L \approx 368$ THz stabilized to a reference cavity that is calibrated by a frequency comb linked to the Sr clock. By applying a volume Bragg grating with a bandwidth of ~ 20 GHz, we suppress amplified spontaneous emission of the lattice laser and reduce the relevant light shift [11] to less than 10^{-19}.

^{87}Sr atoms are laser-cooled to ~ 5 μK and loaded into the lattice with its depth of $u_{\rm ref} = 272$ ($u_{\rm ref} E_R/k_{\rm B} = 45\,\mu$K). This loading condition is kept constant during measurements. A bias magnetic field of $|\mathbf{B}_{\rm bias}| = 65$ μT is applied along the x-axis to define the quantization axis and to separate the Zeeman substates. Lattice, optical pumping and clock laser are all polarized parallel to the bias field, while that of the cooling laser is perpendicular to the bias field so as to be decomposed into $\sigma^{\pm}$ components. Applying the π-polarized pumping laser resonant with the $^1S_0$ ($F = 9/2$) $- {}^3P_1$ ($F = 7/2$) transition [see Fig. 1(b)], the atoms are optically pumped to the outermost Zeeman substates $^1S_0$ ($F = 9/2$, $m_F = \pm 9/2$) used for the clock interrogation. In the following, we discuss the case where we take the $m_F = 9/2$ state as the clock state.

Simultaneously with the optical pumping, we apply Doppler cooling (DPC) for the radial motion with the σ^+ component of the cooling laser on the $^1S_0$ ($F = 9/2$, $m_F = 9/2$) $- {}^3P_1$ ($F = 11/2$, $m_F = 11/2$) transition. Consequently, the radial temperature is reduced to $T_r \approx 2$ μK (correspondingly $\zeta_1(u_{\rm ref}) \approx 0.96$), as

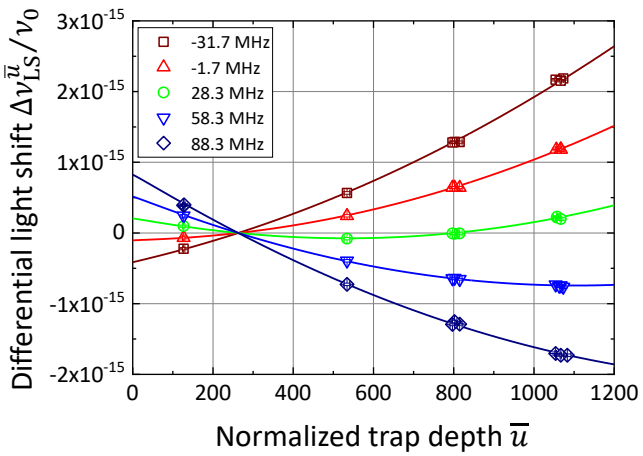

FIG. 2: (color online). Intensity-dependent light shift $\Delta\nu_{\rm LS}^{\bar{u}}$ measured by referencing $\bar{u}_{\rm ref} = 263$. The light shifts are measured at the lattice detunings δ_L as shown in the legend. Error bars give 1σ statistical uncertainties for each measurement. The solid curves fit the measurements according to Eq. (1).

measured by time-of-flight (TOF) thermometry, and the linewidth of the blue-sideband on the clock transition is reduced to ~ 8 kHz as shown in the inset of Fig. 1(c). The atoms remaining in the $m_F = -9/2$ state are heated out of the lattice by the σ^- component of the cooling laser. Subsequently, we apply sideband cooling (SBC) to reduce axial vibrational states to $\bar{n}_z < 0.01$, as measured by the ratio of red and blue sidebands, using the σ^+-polarized cooling-laser propagating along the lattice axis.

In order to purify the m_F state, we excite the atoms to the $^3P_0$ ($m_F = 9/2$) state with a 22-ms-long clock π pulse so as to resolve the Zeeman substates and to select a single m_F state. Atoms in the other Zeeman substates remain unexcited and are subsequently blown away by a laser pulse tuned to the $^1S_0 - {}^1P_1$ transition. For the preparation of atoms in the $^3P_0$ ($m_F = -9/2$) state, we apply the similar procedure with the σ^- component of the cooling laser.

Finally, in order to evaluate the lattice light shift dependence on the trap depth, we adiabatically ramp up or down the lattice depth from $u_{\rm ref}$ to u over 80 ms. Symbols in Fig. 1(c) show reduction factors determined by the TOF measurements, which reasonably follow those assuming adiabatic temperature changes, i.e., $\zeta_j^{\rm ad}(u) = 1 - \frac{1-\zeta_j(u_{\rm ref})}{\sqrt{u/u_{\rm ref}}}$ as shown by dashed lines with corresponding colors. As the reduction factor after the adiabatic ramp is in the range of $0.95 < \zeta_1(u) < 0.99$ for $150 < u < 1150$, we approximate $\overline{w^j} \approx (\zeta_1 u)^j$, which is valid within 0.2% error. The axial vibrational number $\bar{n}_z < 0.01$ is measured unchanged after the adiabatic ramp.

We operate two Sr clocks, Sr1 and Sr2, to evaluate the light shift: Sr1 measures the light shift by varying the lattice depth u or vibrational state n_z of atoms, while Sr2 serves as a frequency anchor. Sr1 and Sr2 simultaneously interrogate the clock transition at $\nu_0 \approx 429$ THz with a common laser to cancel out the Dick effect noise introduced by the clock laser, which improves the Allan deviation for the light shift measurements [28].

Figure 2 shows the intensity-dependent light shift $\Delta\nu_{\rm LS}^{\bar{u}} = \nu_{\rm LS}(\bar{u}, \delta_L, 0) - \nu_{\rm LS}(\bar{u}_{\rm ref}, \delta_L, 0)$ as a function of the effective depth $\bar{u} = \zeta_1(u)u$ by taking $\bar{u}_{\rm ref} = \zeta_1(u_{\rm ref})u_{\rm ref} = 263$ as a reference. We change the lattice laser frequency ν_L every 30 MHz, which are measured with uncertainties less than 100 kHz. The detunings δ_L given in the legend are calculated after determining the E1 magic frequency $\nu^{\rm E1}$ as described below. The hyperpolarizability effect introduces the nonlinear dependence for higher intensity, where we correct the density shift of low 10^{-18} by measuring the density-dependent shift [27].

All the data in Fig. 2 is fitted using the light shift model given in Eq. (1), where we take $\nu^{\rm E1}$, $\frac{\partial\tilde{\alpha}^{\rm E1}}{\partial\nu}$, and $\tilde{\beta}$ as free parameters. As $\tilde{\alpha}^{qm}$ scarcely contributes to this fitting, we conduct another measurements to determine $\tilde{\alpha}^{qm}$ and apply the results to this fitting. We repeat these two fittings until the fitting parameters converge. Finally, the solid fitting curves determine $\nu^{\rm E1} = 368\ 554\ 465.1(1.0)$ MHz, $(\partial\tilde{\alpha}^{\rm E1}/\partial\nu)/h = 1.735(13) \times 10^{-11}$, and $\tilde{\beta}/h = -0.461(14)$ μHz.

As the light shift arising from the multipolar polarizability $\tilde{\alpha}^{qm}$ is sensitive to the vibrational states n_z [18], we measure the differential light shift between $n_z = 1$ and $n_z = 0$ vibrational states given by

$$\begin{aligned} & h\Delta\nu_{\rm LS}^{\rm vib}(u, \delta_L) \\ &= h[\nu_{\rm LS}(u, \delta_L, 1) - \nu_{\rm LS}(u, \delta_L, 0)] \\ &= \left(\frac{\partial\tilde{\alpha}^{\rm E1}}{\partial\nu}\delta_L - \tilde{\alpha}^{qm}\right) u^{1/2} + \tilde{\beta}u\left(2u^{1/2} - 3\right). \end{aligned} \quad (3)$$

This eliminates the otherwise dominating contributions from $\tilde{\alpha}^{\rm E1}$ and $\tilde{\beta}$, and allows extracting $\tilde{\alpha}^{qm}$.

For this measurement, we excite the atoms to the $n_z = 0$ or 1 vibrational state in the $^3P_0$ ($m_F = 9/2$) state by applying a Rapid Adiabatic Passage (RAP) [29] by frequency-sweeping the π-polarized clock laser across the carrier and blue sideband in 6 ms. The Rabi frequency of the clock laser is about 50 kHz (10 kHz) for the carrier (the blue sideband). This RAP allows transferring more than 90% of the atoms to the desired vibrational states. The atoms remaining in the ground state are heated out of the trap by driving the $^1S_0 - {}^1P_1$ transition.

Figure 3 shows the differential light shift $\Delta\nu_{\rm LS}^{\rm vib}(\bar{u}, \delta_L)$ measured for the lattice detuning $\delta_L = 0.4$ MHz. A green line fits the measurements by taking $\tilde{\alpha}^{qm}$ as a free parameter, while $\tilde{\beta}$, $\nu^{\rm E1}$, and $\partial\tilde{\alpha}^{\rm E1}/\partial\nu$ are fixed with the values obtained with the data in Fig. 2. The updated result of $\tilde{\alpha}^{qm}$ is recursively used for deriving the hyperpolarizability. We determine the differential multipolar polarizability to be $\tilde{\alpha}^{qm}/h = -0.962(40)$ mHz. The black dashed line shows $\Delta\nu_{\rm LS}^{\rm vib}(\bar{u}, 0)$ at the E1 magic frequency

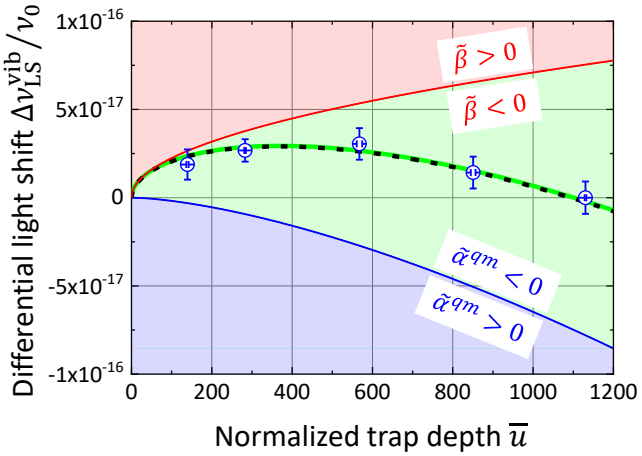

FIG. 3: (color online). Evaluation of the multipolar polarizability from the light shift difference between $n_z = 1$ and $n_z = 0$ measured at $\delta_L = 0.4$ MHz shown by empty circles. Assuming β derived from Fig. 2, regions with $\tilde{\alpha}^{qm} < 0\,(> 0)$ are displayed by upper red/green (lower blue) area. Empty circles fall on the upper region, indicating $\tilde{\alpha}^{qm} < 0$. By taking $\tilde{\alpha}^{qm}$ in Eq. (3) as a free parameter, the fitting determines $\tilde{\alpha}^{qm}/h = -0.962(40)$ mHz as shown by a green line.

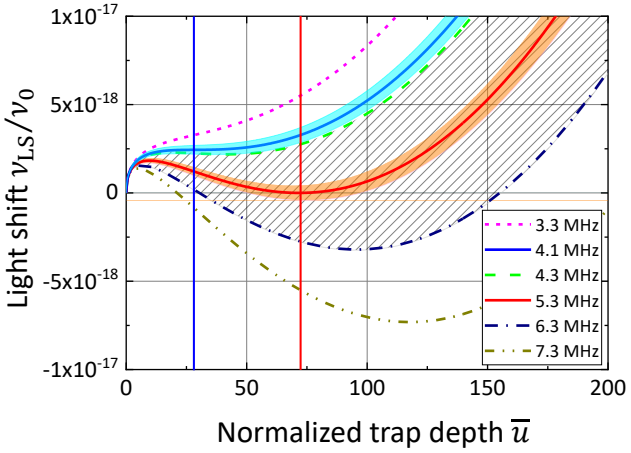

FIG. 4: (color online). Lattice light shift near the operational magic conditions for different detunings δ_L. The red and blue curves show the light shifts for two operational magic frequencies (i) $\delta_L = 5.3(2)$ MHz to make the light shift zero at $\bar{u}^{\rm op} = 72(2)$ (red vertical line), and (ii) $\delta_L = 4.1(1)$ MHz to use an inflection point at $\bar{u}^{\rm op} = 28(1)$ (blue vertical line). Orange (sky-blue) shaded area indicates an uncertainty given by the measured polarizabilities and a hatched area indicates that given by the E1 magic frequency for case (i).

$\nu^{\rm E1}$. By setting $\tilde{\beta} = 0$ and $\tilde{\alpha}^{qm} = 0$, we obtain red and blue lines, which indicate that $\Delta\nu_{\rm LS}^{\rm vib}(\bar{u}, 0)$ is mainly determined by the multipolar polarizability for $\bar{u} < 200$ and the hyperpolarizability starts to contribute for higher intensity. Note that the two lines divide the plot into 3 sections indicated by different colors depending on the signs of these polarizabilities.

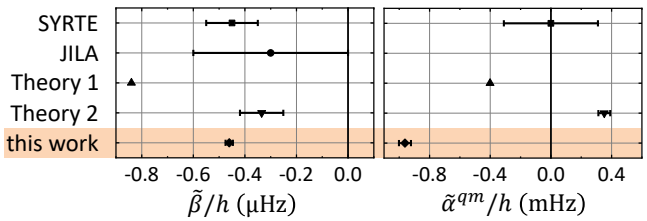

FIG. 5: (color online). Summary of differential hyperpolarizability $\tilde{\beta}$ and multipolar polarizability $\tilde{\alpha}^{qm}$ on the clock transition reported in previous works SYRTE [11, 23], JILA [3], Theory 1 (error bars not available) [21], Theory 2 [22] and this work.

The lattice-induced light shifts $\nu_{\rm LS}(\bar{u}, \delta_L, 0)$ predicted by the obtained polarizabilities are shown in Fig. 4. In addition to making the light shift insensitive to the trap depth $\bar{u}$, i.e., $\frac{\partial \nu_{\rm LS}}{\partial u}|_{u=\bar{u}^{\rm op}} = 0$, the Sr clock transition offers two distinctive operational conditions $(\bar{u}^{\rm op}, \delta_L^{\rm op})$, as it has the same sign for $\tilde{\beta}$ and $\tilde{\alpha}^{qm}$ [27] as indicated by the green area in Fig. 3: (i) by taking $\delta_L^{\rm op} = 5.3(2)$ MHz and $\bar{u}^{\rm op} = 72(2)$, the total light shift can be reduced to less than 1×10^{-19} over the trap depth $60 < u < 83$ as indicated by a red line. Alternatively, (ii) by taking $\delta_L^{\rm op} = 4.1(1)$ MHz and $\bar{u}^{\rm op} = 28(1)$, an inflection point determined by $\frac{\partial^2 \nu_{\rm LS}}{\partial u^2}|_{u=\bar{u}^{\rm op}} = 0$ offers the light shift variation less than 1×10^{-19} over the trap depth $17 < u < 43$ as shown by a blue line. Orange and sky-blue shaded areas indicate the uncertainties of 4×10^{-19} and 2×10^{-19} given by those of measured polarizabilities. The E1 magic frequency uncertainty of 1.0 MHz for the present measurements, including the tensor-shift contribution as discussed in the Supplemental Material [27], gives an overall light-shift uncertainty 3×10^{-18} at $\bar{u}^{\rm op} = 72$ (hatched area) and 1×10^{-18} at $\bar{u}^{\rm op} = 28$, which can be reduced by improving the statistics of the clock measurements. For the lattice depth of $72E_R$ and $28E_R$, the off-resonant lattice-photon scattering rate [30], including Raman scattering in the $^3P_0$ state and Rayleigh scattering, is estimated to be $0.1\,{\rm s}^{-1}$ and $0.04\,{\rm s}^{-1}$, allowing a sufficient clock interrogation time over multiple seconds.

Figure 5 summarizes reported polarizabilities for the $^1S_0 - {}^3P_0$ clock transition of Sr. The hyperpolarizability $\tilde{\beta}$ determined in this work agrees with the previous results [3, 23] within their uncertainties and is close to a recent theory [22]. Our multipolar polarizability $\tilde{\alpha}^{qm}$ deviates from the previous experiment [23] that indicates zero within the uncertainty, and from two theories [21, 22] that give opposite signs with each other.

In summary, we have determined the differential multipolar ($\tilde{\alpha}^{qm}$) and hyper ($\tilde{\beta}$) polarizabilities for Sr optical lattice clocks by precisely controlling the atomic motion. These polarizabilities predict two distinctive operational conditions: the lattice depth and frequency $\delta_L^{\rm op}$ of $(72E_R, 5.3\,{\rm MHz})$ allows cancelling out the lattice light shift and $(28E_R, 4.1\,{\rm MHz})$ allows using the inflec-

tion point, both of which coincide with typical operating conditions for Sr clocks [2, 30]. These operational lattice depth are conveniently described by "magic sideband frequencies" of $\nu_z^{\rm op} = 59(1)/\sqrt{\zeta_1}$ kHz and $29(1)/\sqrt{\zeta_1}$ kHz for the axial motion, respectively, with ζ_1 the intensity reduction factor to be measured. A narrow-line cooling [31] allows $\zeta_1 \approx 0.91$ or better, which well meets the predicted lattice intensity tolerance of more than 30% around the magic intensity. Combined with cryogenic clocks that reduce the blackbody radiation shift [2], the clock uncertainty at the level of 10^{-19} falls within the scope.

We thank M. Das for his contribution to experiments in early stage, N. Ohmae for the operation of comb, and N. Nemitz for careful reading of the manuscripts and valuable comments. This work is supported by JST ERATO Grant Number JPMJER1002 (Japan), by JSPS Grant-in-Aid for Specially Promoted Research Grant Number JP16H06284, and by the Photon Frontier Network Program of the Ministry of Education, Culture, Sports, Science and Technology, Japan.

[1] C. W. Chou, D. B. Hume, J. C. J. Koelemeij, D. J. Wineland, and T. Rosenband, Phys. Rev. Lett. **104**, 070802 (2010).
[2] I. Ushijima, M. Takamoto, M. Das, T. Ohkubo, and H. Katori, Nat. Photonics **9**, 185 (2015).
[3] T. Nicholson, S. Campbell, R. Hutson, G. Marti, B. Bloom, R. McNally, W. Zhang, M. Barrett, M. Safronova, G. Strouse, et al., Nat. Commun. **6**, 6896 (2015).
[4] N. Huntemann, C. Sanner, B. Lipphardt, C. Tamm, and E. Peik, Phys. Rev. Lett. **116**, 063001 (2016).
[5] C. Lisdat, G. Grosche, N. Quintin, C. Shi, S. Raupach, C. Grebing, D. Nicolodi, F. Stefani, A. Al-Masoudi, S. Dörscher, et al., Nat. Commun. **7**, 12443 (2016).
[6] T. Takano, M. Takamoto, I. Ushijima, N. Ohmae, T. Akatsuka, A. Yamaguchi, Y. Kuroishi, H. Munekane, B. Miyahara, and H. Katori, Nat. Photonics **10**, 662 (2016).
[7] J.-P. Uzan, Rev. Mod. Phys. **75**, 403 (2003).
[8] N. Huntemann, B. Lipphardt, C. Tamm, V. Gerginov, S. Weyers, and E. Peik, Phys. Rev. Lett. **113**, 210802 (2014).
[9] A. Derevianko and M. Pospelov, Nat. Phys. **10**, 933 (2014).
[10] S. Kolkowitz, I. Pikovski, N. Langellier, M. Lukin, R. L. Walsworth, and J. Ye, Phys. Rev. D **94**, 124043 (2016).
[11] R. L. Targat, L. Lorini, Y. L. Coq, M. Zawada, J. Guéna, M. Abgrall, M. Gurov, P. Rosenbusch, D. G. Rovera, B. Nagórny, et al., Nat. Commun. **4**, 2109 (2013).
[12] C. Grebing, A. Al-Masoudi, S. Dörscher, S. Häfner, V. Gerginov, S. Weyers, B. Lipphardt, F. Riehle, U. Sterr, and C. Lisdat, Optica **3**, 563 (2016).
[13] F. Riehle, P. Gill, F. Arias, and L. Robertsson, Metrologia **55**, 188 (2018).
[14] H. G. Dehmelt, IEEE Trans. Instrum. Meas. **IM-31**, 83 (1982).
[15] R. C. Brown, N. B. Phillips, K. Beloy, W. F. McGrew, M. Schioppo, R. J. Fasano, G. Milani, X. Zhang, N. Hinkley, H. Leopardi, et al., Phys. Rev. Lett. **119**, 253001 (2017).
[16] H. Katori, M. Takamoto, V. G. Pal'chikov, and V. D. Ovsiannikov, Phys. Rev. Lett. **91**, 173005 (2003).
[17] A. V. Taichenachev, V. I. Yudin, V. D. Ovsiannikov, V. G. Pal'chikov, and C. W. Oates, Phys. Rev. Lett. **101**, 193601 (2008).
[18] H. Katori, K. Hashiguchi, E. Y. Il'inova, and V. D. Ovsiannikov, Phys. Rev. Lett. **103**, 153004 (2009).
[19] A. Brusch, R. LeTargat, X. Baillard, M. Fouché, and P. Lemonde, Phys. Rev. Lett. **96**, 103003 (2006).
[20] H. Katori, V. D. Ovsiannikov, S. I. Marmo, and V. G. Palchikov, Phys. Rev. A **91**, 052503 (2015).
[21] V. D. Ovsiannikov, S. I. Marmo, V. G. Palchikov, and H. Katori, Phys. Rev. A **93**, 043420 (2016).
[22] S. G. Porsev, M. S. Safronova, U. I. Safronova, and M. G. Kozlov, Phys. Rev. Lett. **120**, 063204 (2018).
[23] P. G. Westergaard, J. Lodewyck, L. Lorini, A. Lecallier, E. A. Burt, M. Zawada, J. Millo, and P. Lemonde, Phys. Rev. Lett. **106**, 210801 (2011).
[24] Z. Barber, J. Stalnaker, N. Lemke, N. Poli, C. Oates, T. Fortier, S. Diddams, L. Hollberg, C. Hoyt, A. Taichenachev, et al., Phys. Rev. Lett. **100**, 103002 (2008).
[25] N. Nemitz, T. Ohkubo, M. Takamoto, I. Ushijima, M. Das, N. Ohmae, and H. Katori, Nat. Photonics **10**, 258 (2016).
[26] K. Yamanaka, N. Ohmae, I. Ushijima, M. Takamoto, and H. Katori, Phys. Rev. Lett. **114**, 230801 (2015).
[27] See Supplemental Material for further discussion, which includes Refs. [32-34].
[28] M. Takamoto, T. Takano, and H. Katori, Nat. Photonics **5**, 288 (2011).
[29] J. S. Melinger, S. R. Gandhi, A. Hariharan, J. X. Tull, and W. S. Warren, Phys. Rev. Lett. **68**, 2000 (1992).
[30] S. Dörscher, R. Schwarz, A. Al-Masoudi, S. Falke, U. Sterr, and C. Lisdat, arXiv:1802.02945.
[31] H. Katori, T. Ido, Y. Isoya, and M. Kuwata-Gonokami, Phys. Rev. Lett. **82**, 1116 (1999).
[32] S. Blatt, J. W. Thomsen, G. K. Campbell, A. D. Ludlow, M. D. Swallows, M. J. Martin, M. M. Boyd, and J. Ye, Phys. Rev. A **80**, 052703 (2009).
[33] M. Takamoto, F.-L. Hong, R. Higashi, Y. Fujii, M. Imae, and H. Katori, J. Phys. Soc. Jpn. **75**, 104302 (2006).
[34] M. D. Swallows, M. J. Martin, M. Bishof, C. Benko, Y. Lin, S. Blatt, A. M. Rey, and J. Ye, IEEE Trans. Ultrason. Ferroelectr. Freq. Control **59**, 416 (2012).